Rheologically Tuned Modes of Collective Transport in Active Viscoelastic Films

Henning Reinken* and Andreas M. Menzel†
Institut für Physik, Otto-von-Guericke-Universität Magdeburg, Universitätsplatz 2, 39106 Magdeburg, Germany

(Received 16 February 2025; accepted 22 September 2025; published 29 October 2025)

While many living biological media combine both viscous and elastic properties, most theoretical studies employ either purely fluid or solidlike descriptions. We here use a unified framework for active films on substrates capable of describing a range of viscoelastic behavior to explore the interplay between activity and rheology. The core of the study is a comprehensive state diagram showing a rich world of spatiotemporal dynamic states. Our results demonstrate the potential of tunable rheology to realize modes of controlled active transport on the microscale.

DOI: 10.1103/gbm1-p9cg

Many living biological materials simultaneously exhibit properties of both viscous fluids and elastic solids [1] or may even change their behavior dynamically. For example, during biofilm formation, bacteria excrete extracellular polymeric substances [2,3], which results in complex rheological behavior [4]. Depending on the stage of biofilm formation, the location inside, and the considered timescales, the material is rather fluid or solidlike or somewhere in between. From a physical perspective, such biological systems are described as active matter [5,6], which covers the collective behavior of active, self-propelled agents, frequently embedded in a surrounding medium. However, most studies refer to one of two categories, depending on the considered long-term flow behavior: active fluids or active solids.

Active fluids lack long-term elastic restoring forces and are capable of terminal flow. Primary examples are fluid suspensions of microswimmers [7,8], such as bacteria or artificial self-propelled particles, and active nematics [9]. As described by the seminal Vicsek model [10] and its continuum counterpart, the Toner-Tu theory [11,12], collections of active agents capable of unrestricted long-term movement may develop polar orientational order and directed collective motion. In addition to these flocking or swarming states [13,14], active fluids exhibit various spatiotemporal patterns [15–18] including active turbulence [19–22].

In contrast to active fluids, active solids are unable to support terminal flow due to elastic restoring forces. Instead, they exhibit reversible elastic deformations. In theoretical descriptions, the continuous nature of the embedding medium is often reduced to elastic spring networks of connected active agents [23–27]. Other examples are driven by contractile or extensile active elements and resulting stresses within the medium [28,29], as in muscular tissue [30]. Recent topics of interest in active solids include the nature of excitations [31,32] and the phenomenon of odd elasticity [33,34].

There are numerous theoretical studies on either active solidlike [29,33,35] or active fluidlike materials with simple [12,21,36] or complex [37–43] rheologies. However, a comprehensive exploration of the spatiotemporal dynamics covering these two limiting cases and a continuous spectrum in between is yet to be presented.

We aim to bridge this gap and focus on the interplay of viscous and elastic properties in active media on substrates. To this end, we employ a unified description that can be tuned continuously from the limit of active fluidlike to active solidlike properties. This framework is derived in a companion article [44]. It is motivated from a microscopic picture of active agents and combined with a continuum description of the embedding viscous or (visco)elastic medium. Basic, spatially uniform analytical solutions for resulting dynamic states were obtained for small idealized systems.

Here, we leave this idealization and present a comprehensive dynamical state diagram. It reveals fascinating and novel dynamic states when varying the activity of the suspension and the rheological properties from fluidlike, via viscoelastic, to solidlike. Numerical calculations uncover complex spatiotemporal states, including stripelike patterns in the active viscoelastic regime and separated oscillating domains for increasingly solidlike systems. Moreover, we illustrate how tuning the rheological properties in such active suspensions can be exploited for active collective transport on the microscopic scale. This tuning allows for intermediate storage times, maintaining the spatial arrangement within a set of cargo units.

*Contact author: henning.reinken@ovgu.de
†Contact author: a.menzel@ovgu.de

In short, in the theoretical framework, the behavior is governed by the interplay of three continuum fields [44]. The coarse-grained polar order parameter field $\mathbf{P}$ characterizes the local alignment of active units. It couples to the overall velocity field $\mathbf{v}$ and to the field of elastic displacements $\mathbf{u}$. The latter captures the currently memorized deformation history of the film.

First, the evolution of $\mathbf{P}$ in rescaled units follows as

$$\partial_t \mathbf{P} + \mathbf{v}\cdot\nabla\mathbf{P} = -\mathbf{P} + \nabla^2\mathbf{P} + \mathbf{\Omega}\cdot\mathbf{P} + \gamma_a \mathbf{v}\cdot[(2+\mathbf{P}\cdot\mathbf{P})\mathbf{I}/3 - \mathbf{PP}], \quad (1)$$

where $\mathbf{I}$ is the unit matrix. In addition to advection via the flow field $\mathbf{v}$, Eq. (1) includes reorientation via the vorticity tensor $\mathbf{\Omega} = [(\nabla\mathbf{v})^\top - (\nabla\mathbf{v})]$, where $^\top$ denotes the transpose. The first two terms on the right-hand side arise due to orientational and translational diffusion, while the diffusion coefficients were used to rescale time and space. The term proportional to the alignment strength γ_a captures the tendency of active units to align with the overall flow field $\mathbf{v}$ near a supporting substrate [45–48]. Similar terms are included in various discretized models of active solids [31,49–51]. Nonlinearity limits the magnitude of the polar order parameter to $|\mathbf{P}| \leq 1$.

Second, the velocity field in the low-Reynolds-number limit is determined via the force balance

$$\mathbf{0} = -\nabla p + \eta\nabla^2\mathbf{v} + \mu\nabla^2\mathbf{u} - \nu_v\mathbf{v} - \nu_d\mathbf{u} + \nu_p\mathbf{P}. \quad (2)$$

We here assume an incompressible material, $\nabla\cdot\mathbf{v} = 0$, enforced by the pressure field p. Besides hydrodynamic viscous stress, the equation includes elastic stresses due to previous strain deformations of the material [44,52–54]. Viscosity η and shear modulus μ together with the field of memorized elastic displacements $\mathbf{u}$ quantify these viscous and elastic stresses. Underlying friction with the substrate is set by ν_v and slows down movement. Similarly, elastic restoring forces quantified by ν_d result from interactions with the substrate and pull material elements back to their memorized positions. Active forcing drives the dynamics of the film and is set by ν_p.

Third, the dynamics of $\mathbf{u}$ is governed by

$$\partial_t\mathbf{u} + \mathbf{v}\cdot\nabla\mathbf{u} = \mathbf{v} - \tau_d^{-1}\mathbf{u} - \nabla q. \quad (3)$$

These dynamics result systematically for elastic strain in established generalized hydrodynamic theories that include elasticity [44,52–55]. On the right-hand side, overall motion $\mathbf{v}$ generates displacements $\mathbf{u}$. The field $\mathbf{u}$ is defined via $\mathbf{u}(\mathbf{x},t) = \mathbf{x} - \boldsymbol{a}(\mathbf{x},t)$ [52], where $\mathbf{x}$ indicate the space positions and t the time. $\boldsymbol{a}(\mathbf{x},t)$ describes the "memorized" [56] reference positions that the material elements would relocate to if all elastic stresses at time t were released. Thus, elastic strains are calculated from fixed space positions $\mathbf{x}$ and nonfixed reference positions $\boldsymbol{a}(\mathbf{x},t)$. For viscoelastic materials of incomplete elasticity, the memory of the reference positions $\boldsymbol{a}$ and thus $\mathbf{u}$ may decay with a relaxation time τ_d so that net relocations become permanent. Full elastic reversibility for solids is found in the limit $\tau_d \to \infty$. Finite values τ_d describe viscoelastic fluids, while the limit $\tau_d \to 0$ refers to purely viscous fluids. Thus, rheology can be tuned continuously from fluid to solidlike behavior via τ_d. This description allows to explore a spectrum of viscoelastic substances. Equation (3) includes convective transport $\mathbf{v}\cdot\nabla\mathbf{u}$ by overall flow and, in combination with Eq. (2), represents a first step beyond linear elasticity [56]. It can be derived from a systematic continuum theory [52] based purely on conservation laws and symmetry arguments upon linearization in $\nabla\mathbf{u}$ [44]. The contribution $-\nabla q$ arises from incompressibility $\nabla\cdot\mathbf{u} = 0$ under linearized strains [44].

Previous derivation of the theory suggested three idealized, analytical, spatially uniform mathematical solutions [44]. We here challenge their stability, amended by numerical simulations. For technical details see the Supplemental Material [57]. The central goal is to construct the dynamical state diagram for active films of viscoelastic rheology.

Figure 1 shows a corresponding illustration. There, from bottom to top, we increase the strength of active forcing ν_p, starting from passive systems ($\nu_p = 0$). From left to right, with increasing displacement relaxation time τ_d, we modify the system from rather viscous, fluidlike behavior toward an increasingly elastic, solidlike system. Remaining parameter values, set as indicated in the caption of Fig. 1, integrate the effects mentioned above in a balanced way. Varying these values, the core three-state structure of the state diagram is maintained, while boundaries may be shifted; see Ref. [57] for details.

On the left of Fig. 1, for $\tau_d \to 0$ and fluidlike systems, we recover the generic stationary states. At low activity, this is a macroscopically disordered, isotropic state ($\mathbf{P} = \mathbf{0} = \mathbf{v}$). With increasing activity, it transitions to an orientationally ordered polar state ($\mathbf{P} \neq \mathbf{0} \neq \mathbf{v}$) of straight motion (see the inset on the top left). Both states in the marked regimes are linearly stable [57]. Corresponding phenomenologies are well known, for example, from the Vicsek model [10], the Toner-Tu theory [11,12], and related extensions [18,20,22].

Raising the influence of elasticity by increasing τ_d, we find that both states extend to the right in Fig. 1. Yet, elasticity seems to hinder motion. Illustratively, the elastic restoring forces pin the active agents. Therefore, the phase boundary between polar moving (green) and isotropic resting (yellow) areas turns toward higher activity with increasing elasticity. The phase boundary results from linear stability analysis and is confirmed numerically [57].

The picture changes notably when we increase elasticity at elevated levels of activity from the polar state. Then novel, qualitatively different behavior emerges. It is marked

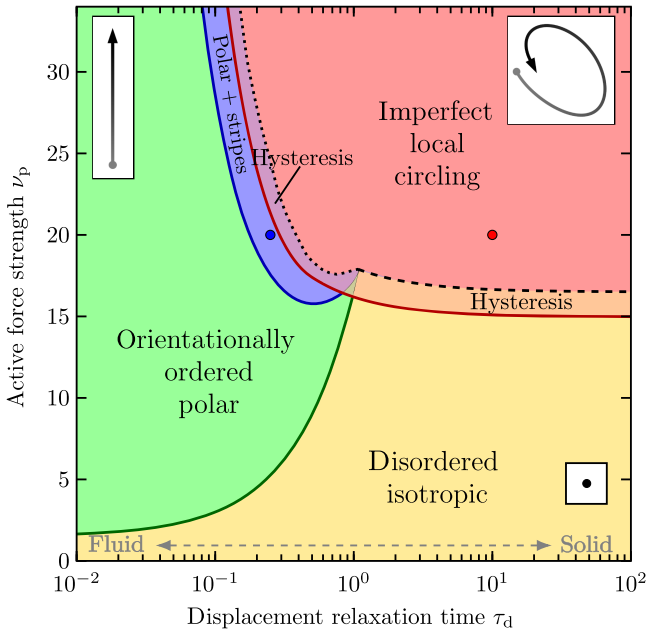

FIG. 1. Dynamical state diagram as a function of the displacement relaxation time τ_d and strength of active forcing ν_p. From left to right, the influence of elasticity increases. Colors indicate regions of different stable dynamical states. Insets in the corners illustrate idealized tracer trajectories. Blue and red dots refer to the dynamical states explored in more detail in Figs. 2 and 3, respectively. Remaining parameter values are $\gamma_a = 1$, $\eta = 1$, $\mu = 1$, $\nu_v = 1$, and $\nu_d = 10$.

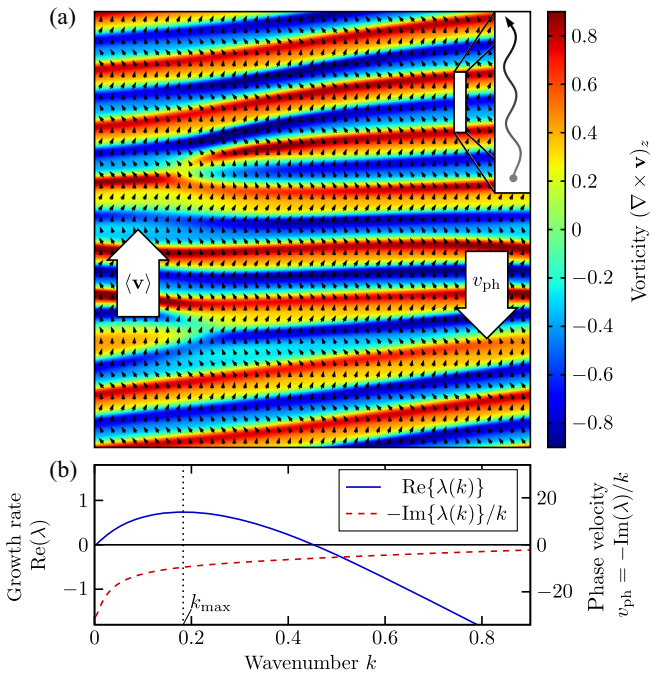

FIG. 2. Stripe pattern associated with the blue region in Fig. 1. (a) Snapshot of the vorticity field $\omega = (\nabla \times \mathbf{v})_z$ in a system of size 200×200 at $\tau_d = 0.25$; see the blue dot in Fig. 1. Small dark arrows indicate the velocity field $\mathbf{v}$. Transport of the patterns, given by the phase velocity $v_{ph} = -\mathrm{Im}\{\lambda(k)\}/k$, is opposite to the averaged active flow direction $\langle \mathbf{v} \rangle$. Associated material trajectories are snakelike; see the top right inset. (b) Largest growth rates $\mathrm{Re}\{\lambda(k)\}$ of modes $\mathbf{k} \| \langle \mathbf{v} \rangle$ when starting from a uniform polar state, and phase velocity $v_{ph} = -\mathrm{Im}\{\lambda(k)\}/k$. Remaining parameter values are $\gamma_a = 1$, $\eta = 1$, $\mu = 1$, $\nu_v = 1$, $\nu_d = 10$, and $\nu_p = 20$.

by the blue region in Fig. 1. Numerical evaluations indicate a stripelike dynamic state; see Fig. 2(a). The inset depicts associated wiggling, snakelike motion.

Indeed, the state of globally uniform polar orientational order becomes linearly unstable in this region [57]. For the associated linear stability analysis [57], we summarize all dynamic quantities in a vector $\mathbf{V}$. We consider small perturbations $\delta\mathbf{V}$ in terms of Fourier modes of wave vector $\mathbf{k}$, $\delta\mathbf{V} = \delta\hat{\mathbf{V}} e^{\lambda t} e^{i\mathbf{k}\cdot\mathbf{x}}$. The growth rate $\mathrm{Re}\{\lambda(k = |\mathbf{k}|)\}$ is plotted in Fig. 2(b), with $\mathbf{k}$ oriented parallel to $\mathbf{P}$. Importantly, the fastest-growing mode is of finite wave number $k_{max} > 0$. Thus, the instability features a certain length scale $\Lambda = 2\pi/k_{max}$, at least close to its onset. This length is reflected by spatial modulations along the migration direction; see Fig. 2(a). There, the local velocity field is indicated by the dark arrows. Its directions deviate periodically in space from the average migration direction given by $\langle \mathbf{v} \rangle$. The periodic modulation is further visualized by the vorticity field $\omega = (\nabla \times \mathbf{v})_z$; see the colored stripe pattern in Fig. 2(a).

Moreover, from $\mathrm{Im}\{\lambda(k)\}$, we calculate the phase velocity of the pattern, $v_{ph} = -\mathrm{Im}(\lambda)/k$. It characterizes the traveling speed of the individual waves. Interestingly, we always find $v_{ph} < 0$. Consequently, the emerging structures travel in the direction opposite to global motion $\langle \mathbf{v} \rangle$; see Fig. 2(a) and Supplemental Movie 1 [57].

Banded structures are observed in various systems of active matter. Examples include traveling density bands in self-propelled particles [61], bands in suspensions of microswimmers subject to external fields [62], or active nematic systems [63]. In contrast to these earlier observations, the traveling bandlike structures we find here at the boundary of the ordered polar state are induced by elasticity, only observable in the viscoelastic regime.

Further increasing the influence of elasticity via τ_d to the right in Fig. 1, we cross the red line. It marks the existence of a basic analytical solution, corresponding to rotating spatially uniform polar order $\mathbf{P}$, flow $\mathbf{v}$, and memorized displacements $\mathbf{u}$ [57]. Yet, we do not observe this state in our spatially extended numerical systems.

Here, numerically, we identify a hysteretic regime until we reach the dotted line in Fig. 1 [57]. In this area, the emergent state depends sensitively on the initial conditions. On the one hand, upon initialization by a weakly perturbed state of global polar orientational order, still the stripe patterns develop. On the other hand, upon initialization by a weak perturbation of the above-mentioned rotational analytical solution [57], rotations of the three fields are

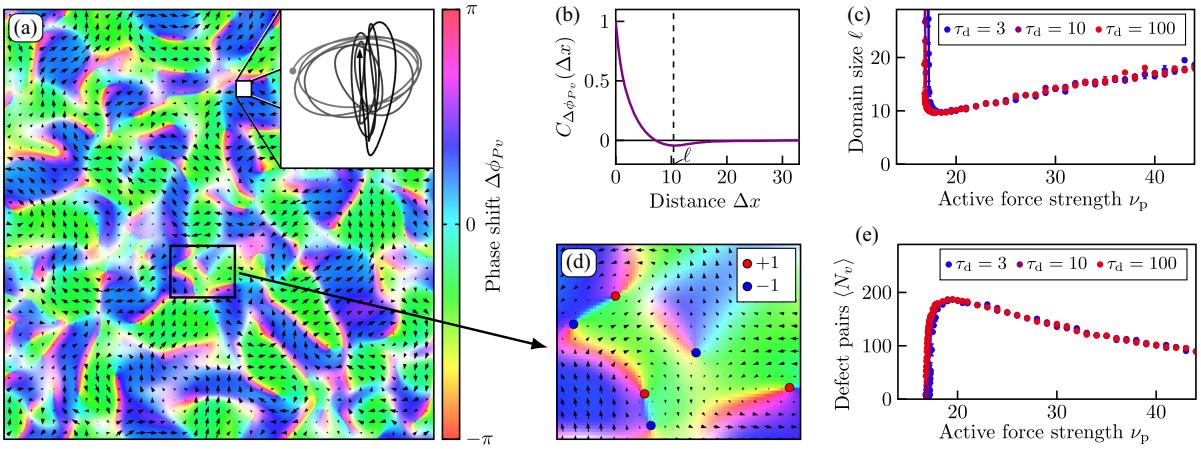

FIG. 3. Heterogeneous state of imperfect local circling motion. (a) At each spot, the vectors of polar orientational order $\mathbf{P}$ and collective flow $\mathbf{v}$ (dark arrows) rotate over time. Domains are identified by the field of phase shift $\Delta\phi_{Pv}$ (color bar) between $\mathbf{P}$ and $\mathbf{v}$. Positive and negative values are connected to clockwise and counterclockwise rotation, respectively. A sample trajectory is shown in the top right corner. The size of the snapshot is 100×100. (b) Averaged spatial correlation function $C_{\Delta\phi_{Pv}}(\Delta x)$ of the phase shift $\Delta\phi_{Pv}$ between any two points of evaluation with distance Δx from each other. The associated characteristic length scale ℓ of the dynamic patterns is identified with the first minimum of $C_{\Delta\phi_{Pv}}(\Delta x)$. (c) Typical domain size ℓ as a function of active force strength ν_p for different values of the relaxation time τ_d. (d) Enlarged view of the marked area in (a) showing $+1$ and -1 defects in the velocity field as red and blue dots. (e) Time-averaged number of defect pairs $\langle N_v \rangle$ in the velocity field of a system of size 200×200 as a function of ν_p. Remaining parameter values are $\gamma_a = 1$, $\eta = 1$, $\mu = 1$, $\nu_v = 1$, $\nu_d = 10$, and $\nu_p = 20$.

maintained. Further to the right of the dotted line in Fig. 1, the stripes are not found as a final dynamic state any more. Although transients can be observed for different initializations, at the end, we find a state of locally rotating fields $\mathbf{P}$, $\mathbf{v}$, and $\mathbf{u}$; see Fig. 3(a). In fact, this state is not spatially uniform. The system splits up into different domains of rotation. It becomes spatially heterogeneous.

Physically, the elastic restoring forces for elevated τ_d become too strong to allow for persistent directed motion as in the globally ordered polar or stripelike states. Thus, these are suppressed by higher levels of elasticity. Instead, local rotations of the polar order $\mathbf{P}$, flow field $\mathbf{v}$, and memorized displacements $\mathbf{u}$ combine active motion with local elastic anchoring. Imperfect circular trajectories arise; see the top right insets in Figs. 1 and 3(a).

The rotations of the fields $\mathbf{P}$, $\mathbf{v}$, and $\mathbf{u}$ are associated with local phase shifts between them. These phase shifts can be used to identify the local domains of rotation; see Fig. 3(a). For example, the field of phase shift $\Delta\phi_{Pv} = \phi_P - \phi_v$ refers to the local angle between $\mathbf{P}$ and $\mathbf{v}$. Remarkably, rotations in different domains may occur with opposite sense of rotation, which is indicated by the different signs in $\Delta\phi_{Pv}$. Supplemental Movie 2 [57] provides a dynamic visualization of the dynamic state associated with the snapshot in Fig. 3(a). From there, it also becomes evident that the domains of correlated phases are constantly evolving in time.

To quantify the length scales of correlated domains, we calculate the equal-time spatial correlation function

$$C_{\Delta\phi_{Pv}}(\Delta x) = \langle \Delta\phi_{Pv}(\mathbf{x}, t)\Delta\phi_{Pv}(\mathbf{x} + \hat{\mathbf{n}}\Delta x, t)\rangle_{\hat{\mathbf{n}},\mathbf{x},t}. \quad (4)$$

Here, Δx is the distance between any two points in space and $\hat{\mathbf{n}}$ is the direction of their separation. $\langle \ldots \rangle_{\hat{\mathbf{n}},\mathbf{x},t}$ denotes the average over orientations $\hat{\mathbf{n}}$, space positions $\mathbf{x}$, and time t. For the dynamically evolving state depicted in Fig. 3(a), we plot $C_{\Delta\phi_{Pv}}(\Delta x)$ in Fig. 3(b). The distinct length scale ℓ quantifying the typical domain size is identified with the location of the first minimum of $C_{\Delta\phi_{Pv}}(\Delta x)$. Indeed, we find that the length scale ℓ of the typical size of the correlated domains is of the same order as the thickness of the stripes $\Lambda/2$ referred to in Fig. 2(a). Figure 3(c) shows ℓ as a function of the strength of active forcing ν_p for different values of the relaxation time τ_d within the red region of Fig. 1. Mainly, we find that ℓ obtains a minimum, but then increases continuously with increasing activity ν_p. Thus, the structures become increasingly correlated. Approaching the transition to the isotropic state (see below), ℓ diverges and the structures are highly correlated in space. Overall, we find that the relaxation time of elasticity in terms of τ_d has only little influence on ℓ for the considered parameters.

As in various other systems of active matter [9,22,64,65], defects in the velocity and polar order parameter fields are continuously pairwise created and annihilated. Their mobility is visualized in Supplemental Movie 3 [57]. In contrast to active nematics [9,64], we observe defects of integer value in our polar system. $+1$ defects correspond to vortices, whereas -1 defects locate (saddle) points in between; see Fig. 3(d). We expect the number of defects to

behave oppositely to the domain size ℓ in Fig. 3(c). Indeed, Fig. 3(e) confirms this relation for the time-averaged number of defect pairs $\langle N_v \rangle$ in the velocity field as a function of activity ν_p for different values of τ_d. The time-averaged number of defect pairs for the field $\mathbf{P}$ yields qualitatively the same result [57].

Finally, we address the transition across the lower boundary of the red region in Fig. 1. Increasing the strength of activity ν_p from the bottom, the isotropic state only becomes linearly unstable at the dashed black line [57]. Indeed, we numerically observe isotropy up to the dashed line for weakly perturbed isotropic initialization. Conversely, dynamic states of circling are found down to the red line, if the system is initialized by the weakly perturbed idealized rotational analytical solution [57]. This scenario reveals a region of hysteresis. A subcritical bifurcation is identified in a simplified analytical approach, as discussed separately for the idealized, spatially uniform analytical solutions [44].

As an immediate perspective, changing the rheology of active films allows to control collective transport. For example, light and external electric fields enable remote dynamic tuning of the rheology of photorheological [66–68] or electrorheological [69] materials. Exploiting such effects facilitates externally controlled transport of cargo by active carrier media. Persistent polar orientational order implies directed transport, while switching to the nonpolar states facilitates intermediate storage. Elevated activity implies increased speed of transport. It requires intermediate switching to the state of imperfect local circling during storage intervals. We numerically demonstrate this scenario in Fig. 4 by periodically changing the relaxation time τ_d; see Fig. 4(a). Resulting trajectories in Fig. 4(b) show the transport of an array of cargo objects, including intermediate storage periods, while maintaining the internal positional order within the array. Suitable preparation of the substrate can guide the transport.

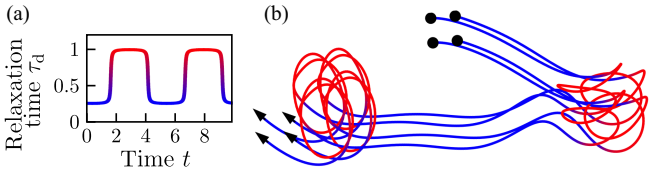

FIG. 4. Rheologically controlled transport of an array of cargo objects. (a) We periodically vary the relaxation time τ_d of elastic displacements between 0.25 and 1. Thus, we tune the degree of elasticity. (b) Resulting trajectories for an array of four transported cargo objects. Tuning rheology allows in a controlled way to switch between persistent collective transport and intermediate storage times, roughly maintaining the spatial order within the transported cargo array. Blue and red parts in (a) and (b) correspond to each other and to the blue and red regions in the state diagram in Fig. 1. The remaining parameters are $\gamma_a = 1$, $\eta = 1$, $\mu = 1$, $\nu_v = 1$, $\nu_d = 10$, and $\nu_p = 20$. The initial edges in the cargo array are of length 1.

The approach opens new routes in microfluidics powered by the activity of microswimmers such as bacteria [70–73]. Instead varying the relaxation time in space suggests a potential mechanism for persistent particle trapping.

In summary, we uncover a rich world of dynamic states that result from the interplay between viscoelasticity and activity. We construct a corresponding overall state diagram. Emergent stripelike patterns are identified between purely viscous active fluids and purely elastic active solids. Their origin is thus different from earlier observed banded structures [61–63]. Heterogeneous states of imperfect local circling result from elastic forces within the system, in contrast to heterogeneous, turbulencelike states observed in purely viscous suspensions of microswimmers [22,65]. Moreover, the elastic pinning and restoring forces are local and internal. Interestingly, circling has been observed experimentally in real systems under elastic pinning at their boundaries or lateral confinement. Examples are model systems of elastic solids [31] or confined human crowds [74]. Together, these observations suggest circling as a general mechanism to balance both effects, active propulsion and elastic pinning or confinement. Future extensions shall include, for example, inertial effects, nonuniform concentrations of active objects, or direct interactions between them at elevated concentrations.

Besides suggesting engineered active systems to control directed transport of cargo on the microscale, our description relates to the complex dynamical behavior in living biological matter. Biofilms and similar collections of cells on substrates show complex flow patterns [75,76], which are reminiscent of the structures observed in Fig. 3(a). Bacterial biofilms [2–4], in particular, may change their rheological characteristics dynamically and continuously from purely viscous via viscoelastic to elastic as a function of time and position within the film.

Generally, we wish to stimulate experimental and theoretical research on biological and artificial active materials that exploit dynamical changes in rheological properties to gain functionality. In this sense, future research may address the further development of adaptive living materials [77], active synthetic systems [78,79], and actuators [80,81]. Our results demonstrate the potential of tunable viscoelasticity to accommodate varying needs and demand during application.

Acknowledgments—We thank the Deutsche Forschungsgemeinschaft (German Research Foundation, DFG) for support through Research Grant Projects No. 413993436 (ME 3571/5-1) and No. 541972050 (ME 3571/12-1). Moreover, A. M. M. acknowledges support through the Heisenberg Grant No. 413993216 (ME 3571/4-1) funded by the Deutsche Forschungsgemeinschaft (German Research Foundation, DFG).

Data availability—The data that support the findings of this article are openly available [82].

[1] G. Li, E. Lauga, and A. M. Ardekani, Microswimming in viscoelastic fluids, J. Non-Newtonian Fluid Mech. **297**, 104655 (2021).

[2] L. Hall-Stoodley, J. W. Costerton, and P. Stoodley, Bacterial biofilms: From the natural environment to infectious diseases, Nat. Rev. Microbiol. **2**, 95 (2004).

[3] V. M. Worlitzer, A. Jose, I. Grinberg, M. Bär, S. Heidenreich, A. Eldar, G. Ariel, and A. Be'er, Biophysical aspects underlying the swarm to biofilm transition, Sci. Adv. **8**, eabn8152 (2022).

[4] S. Jana, S. G. Charlton, L. E. Eland, J. G. Burgess, A. Wipat, T. P. Curtis, and J. Chen, Nonlinear rheological characteristics of single species bacterial biofilms, npj Biofilms Microbiomes **6**, 19 (2020).

[5] M. C. Marchetti, J. F. Joanny, S. Ramaswamy, T. B. Liverpool, J. Prost, M. Rao, and R. A. Simha, Hydrodynamics of soft active matter, Rev. Mod. Phys. **85**, 1143 (2013).

[6] C. Bechinger, R. Di Leonardo, H. Löwen, C. Reichhardt, G. Volpe, and G. Volpe, Active particles in complex and crowded environments, Rev. Mod. Phys. **88**, 045006 (2016).

[7] E. Lauga and T. R. Powers, The hydrodynamics of swimming microorganisms, Rep. Prog. Phys. **72**, 096601 (2009).

[8] J. Elgeti, R. G. Winkler, and G. Gompper, Physics of microswimmers—single particle motion and collective behavior: A review, Rep. Prog. Phys. **78**, 056601 (2015).

[9] A. Doostmohammadi, J. Ignés-Mullol, J. M. Yeomans, and F. Sagués, Active nematics, Nat. Commun. **9**, 3246 (2018).

[10] T. Vicsek, A. Czirók, E. Ben-Jacob, I. Cohen, and O. Shochet, Novel type of phase transition in a system of self-driven particles, Phys. Rev. Lett. **75**, 1226 (1995).

[11] J. Toner and Y. Tu, Flocks herds, and schools: A quantitative theory of flocking, Phys. Rev. E **58**, 4828 (1998).

[12] J. Toner, Y. Tu, and S. Ramaswamy, Hydrodynamics and phases of flocks, Ann. Phys. (Amsterdam) **318**, 170 (2005).

[13] H. Jeckel, E. Jelli, R. Hartmann, P. K. Singh, R. Mok, J. F. Totz, L. Vidakovic, B. Eckhardt, J. Dunkel, and K. Drescher, Learning the space-time phase diagram of bacterial swarm expansion, Proc. Natl. Acad. Sci. U.S.A. **116**, 1489 (2019).

[14] A. Be'er, B. Ilkanaiv, R. Gross, D. B. Kearns, S. Heidenreich, M. Bär, and G. Ariel, A phase diagram for bacterial swarming, Commun. Phys. **3**, 66 (2020).

[15] A. Be'er and G. Ariel, A statistical physics view of swarming bacteria, Mov. Ecol. **7**, 1 (2019).

[16] D. Nishiguchi, I. S. Aranson, A. Snezhko, and A. Sokolov, Engineering bacterial vortex lattice via direct laser lithography, Nat. Commun. **9**, 4486 (2018).

[17] I. S. Aranson, Bacterial active matter, Rep. Prog. Phys. **85**, 076601 (2022).

[18] H. Reinken, S. Heidenreich, M. Bär, and S. H. L. Klapp, Pattern selection and the route to turbulence in incompressible polar active fluids, New J. Phys. **26**, 063026 (2024).

[19] C. Dombrowski, L. Cisneros, S. Chatkaew, R. E. Goldstein, and J. O. Kessler, Self-concentration and large-scale coherence in bacterial dynamics, Phys. Rev. Lett. **93**, 098103 (2004).

[20] H. H. Wensink, J. Dunkel, S. Heidenreich, K. Drescher, R. E. Goldstein, H. Löwen, and J. M. Yeomans, Meso-scale turbulence in living fluids, Proc. Natl. Acad. Sci. U.S.A. **109**, 14308 (2012).

[21] H. Reinken, S. H. L. Klapp, M. Bär, and S. Heidenreich, Derivation of a hydrodynamic theory for mesoscale dynamics in microswimmer suspensions, Phys. Rev. E **97**, 022613 (2018).

[22] R. Alert, J. Casademunt, and J.-F. Joanny, Active turbulence, Annu. Rev. Condens. Matter Phys. **13** (2022).

[23] H. Shen, P. Tan, and L. Xu, Probing the role of mobility in the collective motion of nonequilibrium systems, Phys. Rev. Lett. **116**, 048302 (2016).

[24] E. Ferrante, A. E. Turgut, M. Dorigo, and C. Huepe, Elasticity-based mechanism for the collective motion of self-propelled particles with springlike interactions: A model system for natural and artificial swarms, Phys. Rev. Lett. **111**, 268302 (2013).

[25] C. Hernández-López, P. Baconnier, C. Coulais, O. Dauchot, and G. Düring, Model of active solids: Rigid body motion and shape-changing mechanisms, Phys. Rev. Lett. **132**, 238303 (2024).

[26] P. Baconnier, V. Démery, and O. Dauchot, Noise-induced collective actuation in active solids, Phys. Rev. E **109**, 024606 (2024).

[27] E. Lång, A. Lång, P. Blicher, T. Rognes, P. G. Dommersnes, and S. O. Bøe, Topology-guided polar ordering of collective cell migration, Sci. Adv. **10**, eadk4825 (2024).

[28] R. J. Hawkins and T. B. Liverpool, Stress reorganization and response in active solids, Phys. Rev. Lett. **113**, 028102 (2014).

[29] A. Maitra and S. Ramaswamy, Oriented active solids, Phys. Rev. Lett. **123**, 238001 (2019).

[30] D. Needleman and Z. Dogic, Active matter at the interface between materials science and cell biology, Nat. Rev. Mater. **2** (2017).

[31] P. Baconnier, D. Shohat, C. H. López, C. Coulais, V. Démery, G. Düring, and O. Dauchot, Selective and collective actuation in active solids, Nat. Phys. **18**, 1234 (2022).

[32] L. Caprini, U. Marini Bettolo Marconi, A. Puglisi, and H. Löwen, Entropons as collective excitations in active solids, J. Chem. Phys. **159** (2023).

[33] C. Scheibner, A. Souslov, D. Banerjee, P. Surówka, W. T. Irvine, and V. Vitelli, Odd elasticity, Nat. Phys. **16**, 475 (2020).

[34] M. Fruchart, C. Scheibner, and V. Vitelli, Odd viscosity and odd elasticity, Annu. Rev. Condens. Matter Phys. **14**, 471 (2023).

[35] M. H. Köpf and L. M. Pismen, Non-equilibrium patterns in polarizable active layers, Physica (Amsterdam) **259D**, 48 (2013).

[36] D. Saintillan and M. J. Shelley, Active suspensions and their nonlinear models, C. R. Phys. **14**, 497 (2013).

[37] E. J. Hemingway, A. Maitra, S. Banerjee, M. C. Marchetti, S. Ramaswamy, S. M. Fielding, and M. E. Cates, Active viscoelastic matter: From bacterial drag reduction to turbulent solids, Phys. Rev. Lett. **114**, 098302 (2015).

[38] A. J. T. M. Mathijssen, T. N. Shendruk, J. M. Yeomans, and A. Doostmohammadi, Upstream swimming in microbiological flows, Phys. Rev. Lett. **116**, 028104 (2016).

[39] E. J. Hemingway, M. E. Cates, and S. M. Fielding, Viscoelastic and elastomeric active matter: Linear instability and nonlinear dynamics, Phys. Rev. E **93**, 032702 (2016).
[40] E. L. C. VI M. Plan, J. M. Yeomans, and A. Doostmohammadi, Active matter in a viscoelastic environment, Phys. Rev. Fluids **5**, 023102 (2020).
[41] A. Choudhary, S. Nambiar, and H. Stark, Orientational dynamics and rheology of active suspensions in weakly viscoelastic flows, Commun. Phys. **6**, 163 (2023).
[42] H. Reinken and A. M. Menzel, Vortex pattern stabilization in thin films resulting from shear thickening of active suspensions, Phys. Rev. Lett. **132**, 138301 (2024).
[43] H. Reinken and A. M. Menzel, Self-sustained patchy turbulence in shear-thinning active fluids, Commun. Phys. **8**, 270 (2025).
[44] H. Reinken and A. M. Menzel, companion paper, Unified description of viscous, viscoelastic, or elastic thin active films on substrates, Phys. Rev. E **112**, 045506 (2025).
[45] T. Brotto, J.-B. Caussin, E. Lauga, and D. Bartolo, Hydrodynamics of confined active fluids, Phys. Rev. Lett. **110**, 038101 (2013).
[46] L. P. Dadhichi, A. Maitra, and S. Ramaswamy, Origins and diagnostics of the nonequilibrium character of active systems, J. Stat. Mech. (2018) 123201.
[47] A. Maitra, P. Srivastava, M. C. Marchetti, S. Ramaswamy, and M. Lenz, Swimmer suspensions on substrates: Anomalous stability and long-range order, Phys. Rev. Lett. **124**, 028002 (2020).
[48] S. Liu, S. Shankar, M. C. Marchetti, and Y. Wu, Viscoelastic control of spatiotemporal order in bacterial active matter, Nature (London) **590**, 80 (2021).
[49] B. Szabó, G. J. Szöllösi, B. Gönci, Z. Jurányi, D. Selmeczi, and T. Vicsek, Phase transition in the collective migration of tissue cells: Experiment and model, Phys. Rev. E **74**, 061908 (2006).
[50] K.-D. N. T. Lam, M. Schindler, and O. Dauchot, Self-propelled hard disks: Implicit alignment and transition to collective motion, New J. Phys. **17**, 113056 (2015).
[51] P. Baconnier, O. Dauchot, V. Démery, G. Düring, S. Henkes, C. Huepe, and A. Shee, Self-aligning polar active matter, Rev. Mod. Phys. **97**, 015007 (2025).
[52] H. Temmen, H. Pleiner, M. Liu, and H. R. Brand, Convective nonlinearity in non-Newtonian fluids, Phys. Rev. Lett. **84**, 3228 (2000).
[53] H. Pleiner, M. Liu, and H. R. Brand, Nonlinear fluid dynamics description of non-Newtonian fluids, Rheol. Acta **43**, 502 (2004).
[54] A. M. Menzel, Linear theory of viscoelasticity in a generalized hydrodynamic framework, arXiv:2505.10032.
[55] P. C. Martin, O. Parodi, and P. S. Pershan, Unified hydrodynamic theory for crystals, liquid crystals, and normal fluids, Phys. Rev. A **6**, 2401 (1972).
[56] M. Puljiz and A. M. Menzel, Memory-based mediated interactions between rigid particulate inclusions in viscoelastic environments, Phys. Rev. E **99**, 012601 (2019).
[57] See Supplemental Material, which includes Refs. [58–60], at http://link.aps.org/supplemental/10.1103/gbm1-p9cg for details on the linear stability analysis of the isotropic and globally ordered polar states, for a list of the idealized explicit spatially uniform analytical solutions, for details on the numerical methods, for changes in the state diagram Fig. 1 upon parameter variations, for a description of the supplemental movies, for additional information on topological defects, and for details on the rheological switching function underlying Fig. 4(a).
[58] C. Canuto, M. Y. Hussaini, A. Quarteroni, and T. A. Zang, *Spectral Methods: Evolution to Complex Geometries and Applications to Fluid Dynamics* (Springer, Berlin, Heidelberg, 2007).
[59] D. R. Durran, *Numerical Methods for Fluid Dynamics* (Springer, New York, 2010).
[60] C. R. Harris, K. J. Millman, S. J. Van Der Walt, R. Gommers, P. Virtanen, D. Cournapeau, E. Wieser, J. Taylor, S. Berg, N. J. Smith *et al.*, Array programming with NumPy, Nature (London) **585**, 357 (2020).
[61] J.-B. Caussin, A. Solon, A. Peshkov, H. Chaté, T. Dauxois, J. Tailleur, V. Vitelli, and D. Bartolo, Emergent spatial structures in flocking models: A dynamical system insight, Phys. Rev. Lett. **112**, 148102 (2014).
[62] H. Reinken, S. Heidenreich, M. Bär, and S. H. L. Klapp, Anisotropic mesoscale turbulence and pattern formation in microswimmer suspensions induced by orienting external fields, New J. Phys. **21**, 013037 (2019).
[63] A. Patelli, I. Djafer-Cherif, I. S. Aranson, E. Bertin, and H. Chaté, Understanding dense active nematics from microscopic models, Phys. Rev. Lett. **123**, 258001 (2019).
[64] L. Giomi, M. J. Bowick, X. Ma, and M. C. Marchetti, Defect annihilation and proliferation in active nematics, Phys. Rev. Lett. **110**, 228101 (2013).
[65] N. Rana, R. Chatterjee, S. Ro, D. Levine, S. Ramaswamy, and P. Perlekar, Defect turbulence in a dense suspension of polar, active swimmers, Phys. Rev. E **109**, 024603 (2024).
[66] H. Oh, A. M. Ketner, R. Heymann, E. Kesselman, D. Danino, D. E. Falvey, and S. R. Raghavan, A simple route to fluids with photo-switchable viscosities based on a reversible transition between vesicles and wormlike micelles, Soft Matter **9**, 5025 (2013).
[67] R. Yang, S. Peng, and T. C. Hughes, Multistimuli responsive organogels based on a reactive azobenzene gelator, Soft Matter **10**, 2188 (2014).
[68] I. Tomatsu, K. Peng, and A. Kros, Photoresponsive hydrogels for biomedical applications, Adv. Drug Delivery Rev. **63**, 1257 (2011).
[69] N. Kuznetsov, V. Kovaleva, S. Belousov, and S. Chvalun, Electrorheological fluids: From historical retrospective to recent trends, Mater. Today Chem. **26**, 101066 (2022).
[70] N. Darnton, L. Turner, K. Breuer, and H. C. Berg, Moving fluid with bacterial carpets, Biophys. J. **86**, 1863 (2004).
[71] B. Kaehr and J. B. Shear, High-throughput design of microfluidics based on directed bacterial motility, Lab Chip **9**, 2632 (2009).
[72] M. J. Kim and K. S. Breuer, Microfluidic pump powered by self-organizing bacteria, Small **4**, 111 (2008).
[73] S. P. Thampi, A. Doostmohammadi, T. N. Shendruk, R. Golestanian, and J. M. Yeomans, Active micromachines: Microfluidics powered by mesoscale turbulence, Sci. Adv. **2**, e1501854 (2016).

[74] F. Gu, B. Guiselin, N. Bain, I. Zuriguel, and D. Bartolo, Emergence of collective oscillations in massive human crowds, Nature (London) **638**, 112 (2025).

[75] V. Yashunsky, D. J. G. Pearce, C. Blanch-Mercader, F. Ascione, P. Silberzan, and L. Giomi, Chiral edge current in nematic cell monolayers, Phys. Rev. X **12**, 041017 (2022).

[76] H. Xu, Y. Huang, R. Zhang, and Y. Wu, Autonomous waves and global motion modes in living active solids, Nat. Phys. **19**, 46 (2023).

[77] B. An, Y. Wang, Y. Huang, X. Wang, Y. Liu, D. Xun, G. M. Church, Z. Dai, X. Yi, T.-C. Tang *et al.*, Engineered living materials for sustainability, Chem. Rev. **123**, 2349 (2022).

[78] S. Kim, C. Laschi, and B. Trimmer, Soft robotics: A bioinspired evolution in robotics, Trends Biotechnol. **31**, 287 (2013).

[79] Z. Wu, Y. Chen, D. Mukasa, O. S. Pak, and W. Gao, Medical micro/nanorobots in complex media, Chem. Soc. Rev. **49**, 8088 (2020).

[80] Y. Kim and X. Zhao, Magnetic soft materials and robots, Chem. Rev. **122**, 5317 (2022).

[81] M. Li, A. Pal, A. Aghakhani, A. Pena-Francesch, and M. Sitti, Soft actuators for real-world applications, Nat. Rev. Mater. **7**, 235 (2022).

[82] H. Reinken and A. M. Menzel, Rheologically tuned modes of collective transport in active viscoelastic films (v1.1), Zenodo (2025), 10.5281/zenodo.17055518.